THE JOURNAL OF PHYSICAL CHEMISTRY C

Article

pubs.acs.org/JPCC

Highly Efficient Bienzyme Functionalized Biocompatible Nanostructured Nickel Ferrite–Chitosan Nanocomposite Platform for Biomedical Application

Jay Singh,[†] Appan Roychoudhury,[‡,○] Manish Srivastava,[§] Vidhi Chaudhary,[⊥] Radha Prasanna,[⊥] Dong Won Lee,[†] Seung Hee Lee,[†] and B. D. Malhotra*[,∥,○,‡]

[†]Department of BIN Fusion Technology and Department of Polymer-Nano Science and Technology, Chonbuk National University, Jeonju, Jeonbuk 561-756, Korea

[‡]Department of Science & Technology Centre on Biomolecular Electronics, Biomedical Instrumentation Section, Material Physics and Engineering Division, CSIR-National Physical Laboratory, Dr. K. S. Krishnan Marg, New Delhi 110012, India

[§]Department of Physics, Dehradun Institute of Technology (DIT), School of Engineering, Greater Noida 201308, India

[⊥]Division of Microbiology and Centre for Conservation & Utilization of Blue-Green Algae (CCUBGA), Indian Agricultural Research Institute, New Delhi 110012, India

[∥]Centre for Nano Bioengineering & Spin Tronics, Chungnam National University, 220 Gung-Dong, Yuseong-Gu, Daejeon, 305-764, Korea

[○]Department of Biotechnology, Delhi Technological University, Shahbad Daulatpur, Main Bawana Road, Delhi 110042, India

Supporting Information

ABSTRACT: A new hybrid nanocomposite based on hydrothermally synthesized nanostructured $NiFe_2O_4$ (n-$NiFe_2O_4$) and chitosan (CH) has been explored for bienzyme (cholesterol esterase (ChEt) and cholesterol oxidase (ChOx)) immobilization for application as total cholesterol biosensor. Results of X-ray diffraction (XRD), scanning electron microscopy (SEM), transmission electron microscopy (TEM), Fourier transform infrared (FTIR), Raman spectroscopy (RS) and vibrating sample magnetometer (VSM) studies demonstrate that the ChEt–ChOx/n-$NiFe_2O_4$–CH composite film is successfully synthesized. The obtained ChEt–ChOx/n-$NiFe_2O_4$–CH nanocomposite film shows large specific area, high conductivity, good biocompatibility, fast redox properties and improved antimicrobial activity. The fabricated ChEt–ChOx/n-$NiFe_2O_4$–CH/ITO bioelectrode exhibits largely improved amperometric biosensing performance, i.e., good linearity (5–400 mg/dL), low detection limit (24.46 mg/dL cm^{-2}), high sensitivity of 1.73 μA/(mg/dL cm^{-2}), fast response time of 15s, reproducibility of more than 15 times, shelf life of about 90 days and low Michaelis–Menten constant (K_m) value as 7.05 mg/dL (0.1825 mM). Furthermore, this modified bioelectrode has been utilized for estimation of total cholesterol in human serum samples. This efficient strategy provides new insight into the design of novel flexible electrodes for a wide range of applications in biosensing, bioelectronics, and clinical applications.

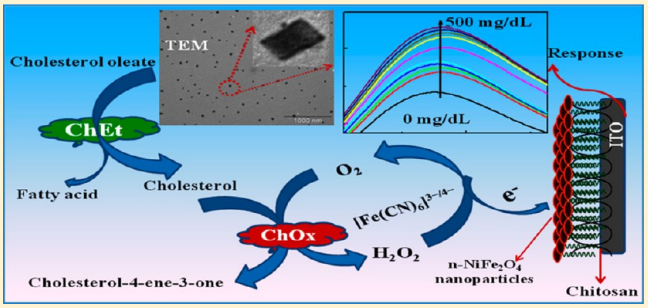

INTRODUCTION

Nanoferrites with general formula MFe_2O_4 have recently opened up new vistas in the frontier field of nanobiomaterial science and nanotechnology because of their remarkable electrical and magnetic properties and many potential applications in spintronics and bioelectronics.[1−4] Among these, application of nanocrystalline ferrites to biosensing has aroused much interest.[5] For medical diagnostics, biosensors can be used to detect glucose, virus, bacteria, neurotoxin, and cholesterol, etc. Among these, cholesterol esterase (ChEt) and cholesterol oxidase (ChOx) based electrochemical biosensors have gained much interest for estimation of total cholesterol level in blood for treatment of clinical disorders including atherosclerosis, hypertension, coronary artery disease, cerebral thrombosis, arteriosclerosis and lipid metabolism dysfunction, etc.[6−8] The principal problem confronting the speedy development of a cholesterol biosensor lies in deep embedment of flavin adenine dinucleotide redox center in the protein core that perhaps prevent direct electrical communication.[9] Another common problem relates to the total number of catalytically active immobilized enzyme units that are known to be small and are randomly oriented resulting in partial denaturation of the immobilized enzyme molecules on the electrode surface. As a result, majority of cholesterol biosensors reported till date do

Received: December 24, 2012
Revised: February 15, 2013
Published: April 12, 2013

not exhibit desired characteristics due to poor biocompatibility of the support matrix.[10] Keeping this in view, many efforts have been made to develop suitable support matrices that may perhaps provide better environment for the efficient immobilization of enzymes and maintenance of the enzymatic bioactivity so as to increase the linearity, detection limit and sensitivity of the biosensor.

Enzyme immobilization has recently gained much interest because the quantity of the desired enzyme is often inadequate due to enzyme instability, high cost, and the limited potential for enzyme recovery.[11,12] The magnetic nanoparticles (MNPs) have recently attracted much attention because of their excellent physical and chemical properties compared to those of conventional bulk materials.[13−17] In this context, ferrites are a group of important magnetic materials that have many efficient technological applications including those in biosensing.[18,19] Nickel ferrite ($NiFe_2O_4$) is known to be an interesting ferrite, due to its technologically important soft inverse spinel structure. Besides this, the nickel ferrite contains improved ferromagnetic properties that originate from magnetic moment of antiparallel spins between Fe^{3+} ions at tetrahedral sites and Ni^{2+} ions at octahedral sites;[20] resulting in high conductivity, lower eddy current loss, high electrochemical stability, good catalytic behavior and also abundance in nature.[21] Additionally, nickel ferrite crystallizes as a spinel structure and exhibits tunable conducting behavior. Because of their large surface-to-volume ratio, high surface reaction activity, high catalytic efficiency and strong adsorption ability, nanonickel ferrites can perhaps be utilized for biosensor applications.[22,23] A recent report relates to the application of $NiFe_2O_4$ for sensing of liquefied petroleum gas.[24] Luo et al. have recently utilized chitosan/$NiFe_2O_4$ nanocomposite film as a suitable matrix for immobilization of enzymes (glucose oxidase and horseradish peroxidase) to obtain better electrocatalytical response to the oxidation of glucose[25] and hydrogen peroxide.[2] $NiFe_2O_4$ nanoparticles show good biocompatibility, noncytotoxicity and easier preparation process,[21] and it can thus be utilized to immobilize ChOx and ChEt.

The biocompatibility of a biomolecule is known to play an important role toward the fabrication of a biosensor. Generally, adsorption of the desired biomolecules directly onto naked surface of a bulk material may result in its denaturation and loss of bioactivity. In this context, increased biocompatibility may perhaps prevent deactivation of the desired biomolecules arising due to surface modification protocol such as adsorption, coating, self-assembly, and graft polymerization etc. However, adsorption of biomolecules onto the surfaces of nanoparticles may perhaps result in retention of the bioactivity because of biocompatibility of the environment. Since *n*-$NiFe_2O_4$ nanoparticles carry high isoelectric point (>IEP, Ni, and Fe oxide phase varying from to 6−10.7, they can electrostatically adsorb enzymes with different charges with the low IEP of enzymes or proteins, making them suitable for biomolecule immobilization. Recently, many researchers have focused on the preparation of novel nanocomposites with good biocompatibility that could be the promising matrices for enzyme immobilization which in turn may result in enhanced selectivity and sensitivity of the desired biosensors. The combination of MNPs with chitosan has been found to play an important role toward the immobilization of biomolecules for biosensor applications due to excellent film-forming ability, high permeability, mechanical strength, nontoxicity, biocompatibility, low cost, and easy availability.[26,7] In this context, the quantitative cytotoxicity tests have recently revealed that both uncoated and chitosan-coated $NiFe_2O_4$ nanoparticles exhibit noncytotoxic behavior.[27,2] The nontoxic and biocompatibility nature of the *n*-$NiFe_2O_4$−CH film may provide suitable platform for biomolecules, for immobilization of enzymes (ChEt and ChOx) resulting in improved electron transfer to the underlying ITO glass substrate. For synthesis of the nanoparticles, low temperature environment is mostly preferred. Some of the physical and chemical methods widely used for the synthesis of nanoferrites relate to ball-milling, sol−gel, coprecipitation, spray pyrolysis, and hydrothermal methods.[28−31] However, the low temperature (200 °C) hydrothermal route of synthesis of nanoferrites may be used to yield well-dispersed, pure and homogeneous nanoparticles.[32]

We report results of the studies relating to the preparation of *n*-$NiFe_2O_4$ via one-step process using hydrothermal technique. The uniform nanocomposite film comprising of *n*-$NiFe_2O_4$ and chitosan has been fabricated onto indium tin oxide (ITO) glass substrate via solution casting. The characterization of the *n*-$NiFe_2O_4$−CH modified thin film has been accomplished using FTIR, scanning electron microscopy (SEM), X-ray powder diffraction (XRD) and Raman spectroscopy studies. The cholesterol biosensor has been constructed by immobilizing ChEt and ChOx onto *n*-$NiFe_2O_4$−CH/ITO nanocomposite electrode. Antimicrobial and seed germination tests of *n*-$NiFe_2O_4$−CH nanocomposite and ChEt−ChOx/*n*-$NiFe_2O_4$−CH nanobiocomposite conducted using the disc diffusion method, reveal strong activity against the common pathogens and crops indicating biocompatibility of the nanocomposite. The optimized experimental conditions for the fabrication and operation of the cholesterol biosensor have also been established. The resulting biosensor can be used for estimation of total cholesterol in clinical samples and has many advantages such as good antimicrobial activity, biocompatibility, high sensitivity, good repeatability, and reproducibility.

EXPERIMENTAL SECTION

Materials. Nickel nitrate hexahydrate $Ni(NO_3)_2{\cdot}6H_2O$, iron nitrate $Fe(NO_3)_3{\cdot}9H_2O$, glacial acetic acid ($C_2H_4O_2$) (70%), ammonia solution (NH_3) (25%), and sodium hydroxide pellets (NaOH) have been purchased from MERCK (New Delhi, India). Chitosan powder (85% deacetylation, low molecular weight), cholesterol oxidase (EC 1.1.36 from *Pseudomonas fluorescens* with specific activity of 26.4 U mg^{-1}), cholesterol esterase (EC 232.808.6 from *P. fluorescens* with specific activity of 13.13 U mg^{-1}), horseradish peroxidise (HRP, 316 U mg^{-1}), O-dianisidine (1%) dye, cholesterol oleate ($C_{45}H_{78}O_2$), and Brij solution (polidocanol) have been procured from Sigma−Aldrich (USA). The stock solutions of ChOx and ChEt (2 mg/mL) and HRP (1 mg/mL) are freshly prepared in phosphate buffer (50 mM, pH 7.0). The cholesterol oleate solution is prepared in 1% Brij solution (polidocanol) prior to use. The indium−tin−oxide (ITO) coated glass (Balzers) sheet of resistance of 15 Ω/cm is used as the substrate for deposition of the desired nanocomposite and serves as the working electrode. All solutions in these studies have been prepared with deionized water of resistivity not less than 18 MΩ cm taken from a Milli-Q water purification system (Milli-Q, USA).

Characterization. Fourier transform infrared (FTIR) spectrophotometer (PerkinElmer, Spectrum BX II) has been used to characterize desired samples in the range of 400−4000 cm^{-1}. The UV−visible spectroscopic studies have been conducted using UV/vis/NIR spectrometer (PerkinElmer,

dx.doi.org/10.1021/jp312698g | J. Phys. Chem. C 2013, 117, 8491−8502

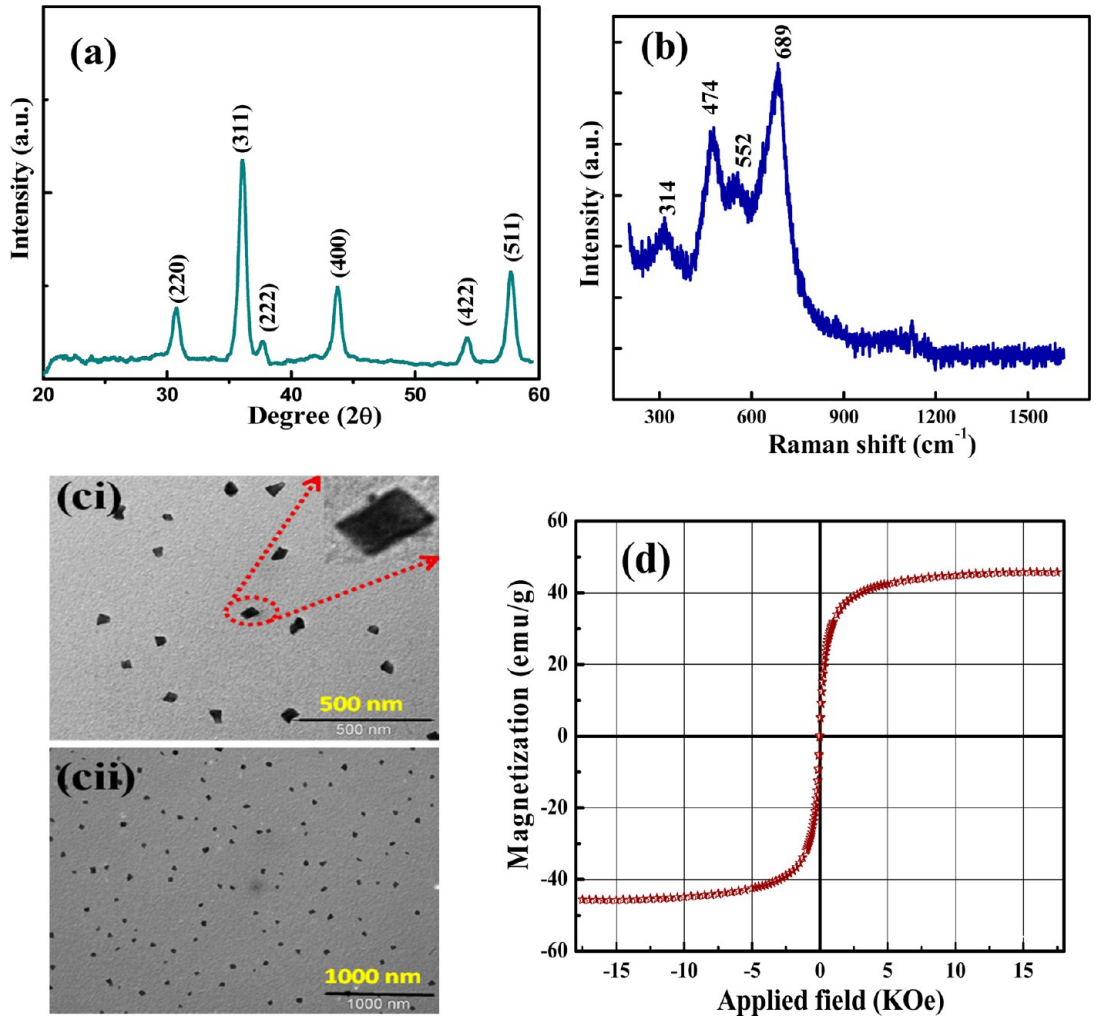

Figure 1. (a) X-ray diffraction pattern, (b) Raman spectrum, (c) TEM images, and (d) VSM (M-H) curves of *n*-$NiFe_2O_4$ nanoparticles.

Lamda 950). Raman spectra have been recorded in the range of 200−2000 cm^{-1} at room temperature (25 °C), using a Renishaw Instruments Raman spectrometer equipped with a high-performance charged coupled device (CCD) detector. The 514 nm of argon-ion laser has been used to illuminate the sample. The surface morphological studies of CH/ITO film, *n*-$NiFe_2O_4$−CH/ITO film and ChEt−ChOx/*n*-$NiFe_2O_4$−CH/ITO bioelectrodes have been investigated using scanning electron microscope (LEO-440). The particle size and shape have been determined via transmission electron microscope (TEM) studies (Hitachi Model H-800 instrument). The X-ray diffraction (XRD) (Rigaku) studies have been used to characterize the $NiFe_2O_4$ nanoparticles using 1.5405 Å Cu Kα as the reference. The hysteresis loop, saturation magnetization and coercivity of the nanocrystalline $NiFe_2O_4$ nanoparticles have been measured by VSM (ADE-DMS, Model EV-7USA) at a maximum applied field of 1.75 T at room temperature (25 °C). The cyclic voltammetry (CV), electrochemical impedance spectroscopy (EIS) and amperometric measurements have been recorded via an Autolab Potentiostat/Galvanostat (Eco Chemie, The Netherlands). The electrochemical measurements have been conducted by using a three-electrode system with ChEt−ChOx/*n*-$NiFe_2O_4$−CH/ITO bioelectrode as the working electrode, a platinum (Pt) wire as the counter electrode, and saturated Ag/AgCl electrode as a reference electrode in phosphate buffer (50 mM, pH 7.0, 0.9% NaCl) containing 5 mM $[Fe(CN)_6]^{3-/4-}$ as a mediator.

Preparation of *n*-$NiFe_2O_4$ Nanoparticles. The nanocrystalline $NiFe_2O_4$ nanoparticles have been prepared via hydrothermal method according to the method reported elsewhere[27] with some modification. The stoichiometric molar amounts of $Ni(NO_3)_2{\cdot}6H_2O$ and $Fe(NO_3)_3{\cdot}9H_2O$ are dissolved in deionized water to prepare uniform solution by stirring. An aqueous solution of ammonia (25%) is added dropwise into this solution in a Teflon-lined stainless steel autoclave with steady stirring (2 h), until pH of the final solution reaches 7−8, when a precipitate is formed. The autoclave is then placed in an oven and is kept at 180 °C for about 15 h after which, the autoclave is allowed to cool to the room temperature. The resulting brown precipitate is washed several times with deionized water and absolute ethanol to eliminate the presence of nitrate ions. The solid product is heated to 90 °C and is dried under vacuum for about 3 h. The proposed reaction mechanism for the formation of pure $NiFe_2O_4$ nanoparticles is shown in eqs 1−3.

$$2Fe(NO_3)_3 + Ni(NO_3)_2 + 8NH_4OH \rightarrow 2Fe(OH)_3 + Ni(OH)_2 + 8NH_4NO_3 \quad (1)$$

$$2Fe(OH)_3 + Ni(OH)_2 \rightarrow NiO + Fe_2O_3 + 4H_2O \quad (2)$$

dx.doi.org/10.1021/jp312698g | J. Phys. Chem. C 2013, 117, 8491−8502

$$NiO + Fe_2O_3 \rightarrow NiFe_2O_4 \quad (3)$$

Preparation of *n*-$NiFe_2O_4$–CH Nanocomposite Film. First 1 g of chitosan (CH) powder is added into 100 mL of 0.1 M acetic acid, and the mixture is stirred to form a 1 wt % clear CH solution. The calculated amount of (30 mg) of *n*-$NiFe_2O_4$ nanoparticles is dispersed into 5 mL of CH solution with stirring at room temperature (25 °C) followed by ultrasonication for about 2 h to get a highly viscous CH solution with uniformly dispersed $NiFe_2O_4$ nanoparticles. The nanocomposite thin film is fabricated by uniformly spreading a 15 μL solution of *n*-$NiFe_2O_4$/CH nanobiocomposite onto an ITO-coated glass surface (0.25 cm^2) and is dried for 12 h at room temperature in a controlled environment after which it is washed with deionized water to remove any unbound particles. It has been found that the optimized ratio of CH solution and $NiFe_2O_4$ nanoparticles taken as 4:1 and 15 μL of *n*-$NiFe_2O_4$/CH solution, uniformly dispersed onto ITO surface to prepare the *n*-$NiFe_2O_4$/CH nanocomposite film, exhibits maximum amperometric current.

Immobilization of ChOx and ChEt on *n*-$NiFe_2O_4$–CH Nanocomposite Film. Freshly prepared solution comprising of ChOx (2 mg/mL) and ChEt (2 mg/mL) taken in the same ratio (1:1) in phosphate buffer (50 mM, pH 7.0) is uniformly spread (10 μL) onto the desired *n*-$NiFe_2O_4$–CH/ITO nanocomposite electrode. The ChEt–ChOx/*n*-$NiFe_2O_4$–CH/ITO bioelectrode is kept undisturbed in a humid chamber for about 12 h at room temperature (25 °C). The ChEt–ChOx/*n*-$NiFe_2O_4$–CH/ITO bioelectrode is washed thoroughly with phosphate buffer (50 mM, pH 7.0) containing 0.9% NaCl to remove any unbound enzyme molecules and is stored at 4 °C when not in use.

Biocompatibility Test. The effect of *n*-$NiFe_2O_4$/CH and ChEt–ChOx/*n*-$NiFe_2O_4$/CH solution on the germination of seeds of mustard and tomato crops has been evaluated using standard germination assay. The seeds are surface sterilized with 0.1% (v/v) mercuric chloride for 30 min, washed with deionized water, soaked in water overnight are kept in an incubator at 17 and 24 °C, respectively. First, 5 mL of 1.2% water agar is poured as medium in each well of 12 wells plates. Three seeds are kept in each well for desired treatment. Then 10 μL of the CH, *n*-$NiFe_2O_4$/CH and ChEt–ChOx/*n*-$NiFe_2O_4$/CH solution are used for testing. The distilled water is used as a control for each plate. The plates of mustard and tomato seeds are kept in an incubator at 17 and 24 °C, respectively. Those observations are taken regularly up to 72 h of incubation period.

RESULTS AND DISCUSSION

Structural and Morphological Studies (X-ray Diffraction). The XRD pattern (Figure 1a) of hydrothermally prepared $NiFe_2O_4$ nanoparticles show reflection planes, (2 2 0), (3 1 1), (2 2 2), (4 0 0), (4 2 2), and (5 1 1), indicating presence of the cubic spinel structure.[33] These diffraction lines provide clear evidence of the formation of the pure $NiFe_2O_4$ nanoparticles when compared with the reported values (JCPDS file number: 10–325). No other phases are seen indicating phase purity of the $NiFe_2O_4$ sample. The average crystallite diameter (d) has been calculated using the Scherrer's equation, from the full width at half-maximum (FWHM) of the diffraction peaks.

$$d = \frac{0.9\lambda}{\beta \cos\theta} \quad (4)$$

where β is the broadening of diffraction peaks measured at half-maximum intensity (radians) and λ = 1.5406 Å, the wavelength of CuKα. The lattice constant of the $NiFe_2O_4$ nanoparticles has been determined using eq 5

$$a = d_{hkl}\sqrt{(h^2 + k^2 + l^2)} \quad (5)$$

The crystallite size estimated from the Scherrer's equation is found to be as ∼7–14 nm and the lattice parameters of $NiFe_2O_4$ are found to be as $a = b = c = 0.84034 \pm 0.00351$ nm.

Raman Studies. According to the classical lattice vibration theory, there is a strong correlation between the crystal structure and the lattice vibrations, and hence physical insight can be obtained via infrared and Raman spectroscopic studies. It appears that during synthesis of the *n*-$NiFe_2O_4$, the formation of other phases such as Fe_3O_4, α-Fe_2O_3, and γ-Fe_2O_3 phases is also possible. Raman spectroscopy has been used to differentiate the *n*-$NiFe_2O_4$ phase from other possible phases such as Fe_3O_4 and γ-Fe_2O_3 that have similar spinel structures and consequently similar XRD patterns.[34,35] Most Raman peaks found in the spectra of *n*-$NiFe_2O_4$ ferrite are close to those of γ-Fe_2O_3. However, it exhibits much stronger peaks at ∼1370 cm^{-1} and ∼1580 cm^{-1} than those of *n*-$NiFe_2O_4$ ferrite.[34,35] No Raman peaks are observed in the range of 1300–1600 cm^{-1}, indicating absence of γ-Fe_2O_3 phase in the synthesized nanoparticles.

The *n*-$NiFe_2O_4$ has a cubic inverse-spinel structure belonging to the space group O_h^7 ($Fd\,3^-m$).[36] The group theory predicts the following vibrational modes in spinel:

$$\Gamma(AB_2O_4) = A_{1g}(R) + E_g(R) + T_{1g}(in) + 3T_{2g}(R) + 2A_{2u}(in) + 2E_u(in) + 4T_{1u}(ir) + 2T_{2u}(in) \quad (6)$$

where (R), (IR), and (in) represent Raman and infrared-active vibrations and inactive modes, respectively.

It has been found that *n*-$NiFe_2O_4$ exhibits five Raman active modes ($A_g + E_g + 3T_{2g}$) and four infrared active modes ($4T_{1u}$). A strong band in the spectral range 670–710 cm^{-1} is a common feature of the Raman spectra of the inverse spinel.[37] This behavior is observed irrespective of the chemical nature of the divalent cations. These bands may be assigned to stretching vibrations of the Fe_3O_4 tetrahedral,[37,38] whereas A_{1g} modes observed in the region, 460–640 cm^{-1} might be assigned to motions of $Fe^{(6+)}O_6$ octahedral.[37] The Raman spectrum of the $NiFe_2O_4$ is shown in Figure 1b. The observed Raman peaks are in good agreement with those reported in the literature.[39,40]

Transmission Electron Microscopic (TEM) Studies. Figure 1ci,ii shows TEM image of the semispherical *n*-$NiFe_2O_4$ nanoparticles. The nanoparticles are monodispersed and are uniformly distributed without aggregation. The average size of the particles is found to be as 25–30 nm.

Magnetic Measurements. The M–H plot obtained from VSM studies as a function of applied magnetic field for hydrothermally synthesized *n*-$NiFe_2O_4$ nanoparticles is shown in Figure 1d. It can be seen that it exhibits typical characteristics of superparamagnetic behavior of *n*-$NiFe_2O_4$ nanoparticles. Besides this, the observed saturation magnetization (M_s) of 46 Am^2/kg, absence of hysteresis loop and nearly immeasurable coercivity and remanence are obtained. No remanence is detected indicating a superparamagnetic beaviour, which is

dx.doi.org/10.1021/jp312698g | J. Phys. Chem. C 2013, 117, 8491–8502

useful for separating magnetic particles from the solution using the external magnetic field. The superparamagnetic behavior of n-$NiFe_2O_4$ nanoparticles suggests that the particles have a single domain structure due to very small size of the nanoparticles.

FTIR Studies. The FT-IR spectra of nanocrystalline $NiFe_2O_4$ nanoparticles, CH/ITO film, n-$NiFe_2O_4$–CH/ITO film, and ChEt–ChOx/n-$NiFe_2O_4$–CH/ITO bioelectrodes are shown in Figure 2ai–iv in the range, 400–4000 cm^{-1}. It shows

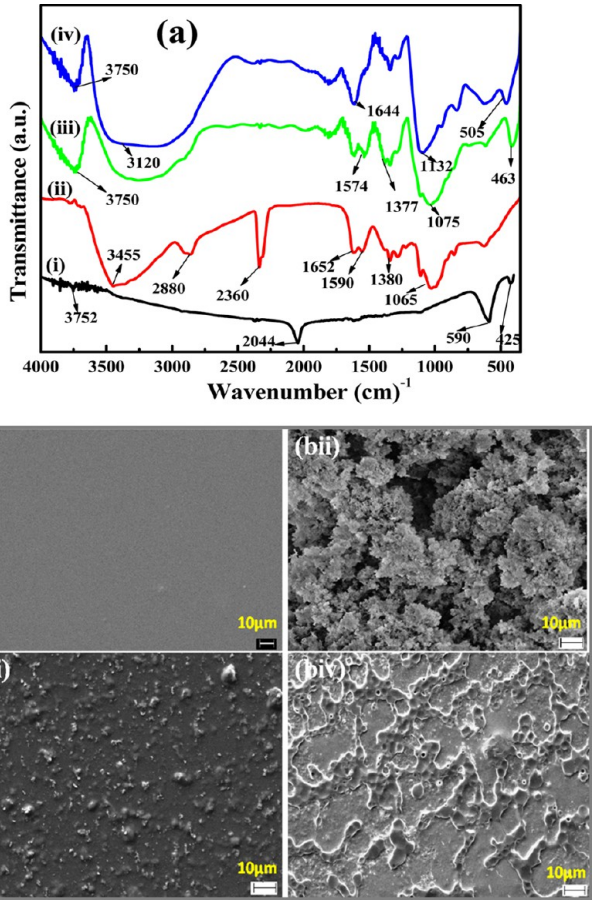

Figure 2. (a) FTIR transmission spectra of (i) $NiFe_2O_4$ nanoparticles, (ii) CH/ITO film, (iii) n-$NiFe_2O_4$–CH/ITO film, and (iv) ChEt–ChOx/n-$NiFe_2O_4$–CH/ITO bioelectrodes. (b) SEM images of CH/ITO film (i), $NiFe_2O_4$ nanopowder (ii), n-$NiFe_2O_4$–CH/ITO film (iii), and ChEt–ChOx/n-$NiFe_2O_4$–CH/ITO bioelectrodes (iv). Scale bar corresponds to 10 μm.

two main broad metal–oxygen bands indicating presence of spinels and ferrites. The FTIR spectra of n-$NiFe_2O_4$ (curve i) exhibits weak bands at 3437 cm^{-1} corresponding to O–H stretching due to physically adsorbed water and two characteristic absorption bands at 424 and 590 cm^{-1}, pertaining to octahedral and tetrahedral sites of positive ions of nickel ferrite, respectively.[41] The difference in the absorption position of octahedral and tetrahedral complexes of $NiFe_2O_4$ crystal is due to different distance between Fe^{3+}–O^{2-} in the octahedral and tetrahedral sites. The FTIR spectrum (curve ii) of CH/ITO electrode exhibits characteristic absorption bands of amino saccharide at 3455 cm^{-1} arising due to overlapping of –OH and $-NH_2$ bands. The 2923 and 2880 cm^{-1} are due to CH_2 stretching and 1652 and 1590 cm^{-1} for carbonyl stretching (C═O) band of amide I and amide II. The peak seen at 1380 cm^{-1} is assigned to –C–O stretching mode of $-CH_2-OH$ groups and 1065 cm^{-1} stretching vibration of C–O–C in glucose circle and 1080–1020 cm^{-1} bands correspond to CH–OH in cyclic compounds. The FTIR spectra of the n-$NiFe_2O_4$–CH/ITO electrode (curve iii) exhibits characteristic IR bands of the functional group corresponding to pure CH (curve ii) and additional band found at 521 and 461 cm^{-1} indicate formation of the M–O band. This suggests that the M–O–M inorganic network is bonded with CH macromolecules via both hydrogen bonding and ionic bonding in the n-$NiFe_2O_4$/ITO electrode. The presence of CH in $NiFe_2O_4$ composite facilitates immobilization of biomolecules via amine and hydroxyl group. However, ChEt–ChOx/n-$NiFe_2O_4$–CH/ITO bioelectrode (curve iv) shows broadening of the peak at 3120 and 1644 cm^{-1} due to addition of carbonyl and amino groups of CH, 1557 cm^{-1} corresponding to C–N stretching and N–H bending modes of amide I band, the 1132 cm^{-1} is due to C–O stretching due to presence of amide bands in protein revealing immobilization of enzymes onto n-$NiFe_2O_4$–CH/ITO nanocomposite matrix via electrostatic interactions.

Scanning Electron Microscopic (SEM) Studies. Surface morphological studies of CH/ITO film, $NiFe_2O_4$ nanoparticles, n-$NiFe_2O_4$–CH/ITO electrode and ChEt–ChOx/n-$NiFe_2O_4$–CH/ITO bioelectrodes have been investigated using SEM and are shown in Figure 2bi-iv. The CH/ITO film (image i) shows homogeneous with relatively smooth and crack-free surface. The SEM image of nanocrystalline $NiFe_2O_4$ nanoparticles (image ii) shows the surface to be rough and particles are agglomerated to each other due to high surface charge of $NiFe_2O_4$. The SEM image of n-$NiFe_2O_4$–CH/ITO film surface (image iii) shows granular and fibrous nanoporous morphology embedded uniformly in the porous chitosan matrix with minimum aggregation. It looks as if some of $NiFe_2O_4$ nanoparticles perhaps agglomerate and CH perhaps bridges the individual $NiFe_2O_4$ particles. However, on the immobilization of ChEt and ChOx, the granular and fibril spherical morphology of n-$NiFe_2O_4$–CH/ITO film changes into the homogeneous globular porous morphology due to presence of ionic interactions between n-$NiFe_2O_4$ and biomolecules, indicating immobilization of enzyme (image iv). Moreover, this fibrous network of n-$NiFe_2O_4$–CH/ITO film provides increased surface area for the immobilization of biomolecules resulting in high enzyme loading.

Biocompatibility and Antimicrobial Test. The observations pertaining to the effect of n-$NiFe_2O_4$/CH and ChEt–ChOx/n-$NiFe_2O_4$/CH on mustard and tomato seed germination shown in Figure 3, parts a and b, respectively, reveal desired seed germination, of the plant tissue culture, indicating biocompatible nature of the nanocomposite. The germinated seeds are counted for each treatment and expressed as % of germination as shown in Table 1. The length of germinated seedlings has been measured and compared for each treatment. All treatments are taken in triplicate. These findings of antimicrobial and biocompatibility activity of n-$NiFe_2O_4$/CH and ChEt–ChOx/n-$NiFe_2O_4$/CH are helpful to maintain the biological activity of enzyme and provide improved platform for in vivo studies.

The antimicrobial studies have been conducted by investigating the development of inhibition zone regularly up to 72 h incubation period in different algal/fungal/bacterial strains shown in Supporting Information (Figure S1). The retardation of inhibition zone is taken as the positive sign indicating biosafety of n-$NiFe_2O_4$/CH modified bioelectrode

dx.doi.org/10.1021/jp312698g | J. Phys. Chem. C 2013, 117, 8491–8502

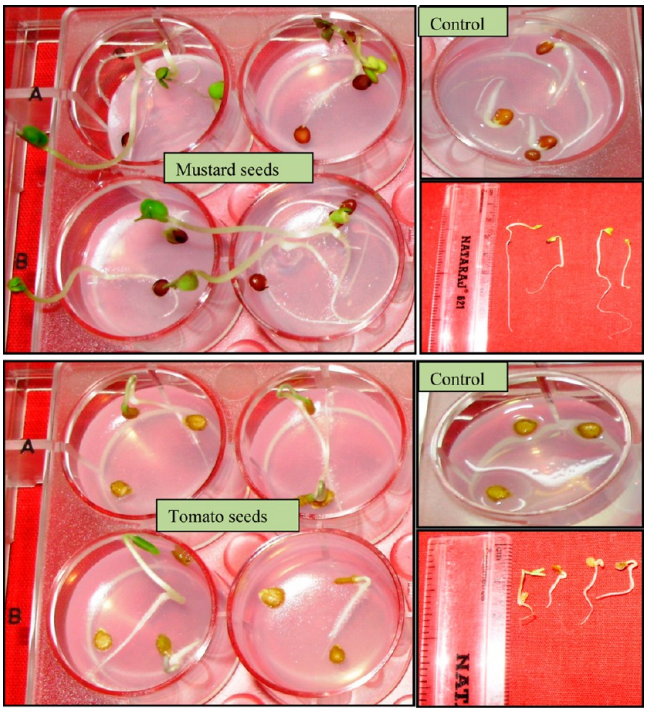

Figure 3. Snapshot of the seed (mustard and tomato) germination in the plant tissue culture using *n*-$NiFe_2O_4$–CH (a) and ChEt–ChOx/*n*-$NiFe_2O_4$–CH (b) solution (0.1%), seeds after 4 days of incubation, revealing proper seed germination, showing the biocompatibility of *n*-$NiFe_2O_4$–CH and ChEt–ChOx/*n*-$NiFe_2O_4$–CH nanocomposite.

Table 1. Bioassay of *n*-$NiFe_2O_4$/CH (A) ChEt–ChOx/*n*-$NiFe_2O_4$/CH (B) and Control (C) against Tomato and Mustard Seeds[a]

		seeds			
		mustard		tomato	
sample no.	sample	% of germination	seedling length (cm)	% of germination	seedling length (cm)
A	CH/*n*-$NiFe_2O_4$ solution (0.1%)	49.995	9.05	49.995	2.25
			3.45		
B	ChEt–ChOx/ *n*-$NiFe_2O_4$/ CH solution (0.1%)	83.33		83.33	2.95
C	control	33.33	11.8	49.995	3.55

[a]Observations: After 48 h, 10 μL samples have been used; average of 5 seeds in replicates.

on the microorganism culture which is shown in Supporting Information (Table S2).

Electrochemical Studies. Figure 4a shows results of the cyclic voltammetry (CV) studies revealing that magnitude of peak current (0.24 mA) of CH/ITO electrode (curve ii) is enhanced as compared to that of the bare ITO electrode (curve i, 0.13 mA) .This can be attributed to the presence of positive charges of CH that are favorable for interaction of ferricyanide anions. Thus, increased number of $[Fe(CN)_6]^{3-/4-}$ ions are attracted to the electrode surface modified with positively charged CH due to presence of electrostatic interactions resulting in increased peak current. After incorporation of $NiFe_2O_4$ nanoparticles into CH matrix, the oxidation peak

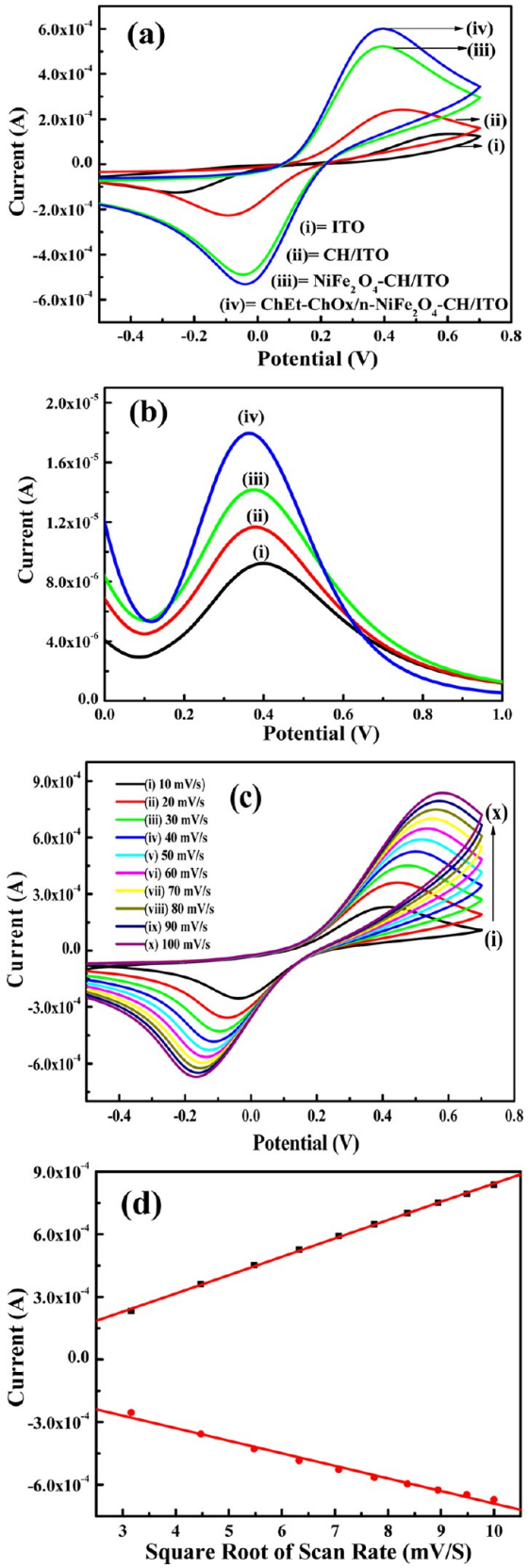

Figure 4. (a) CV and (b) DPV of bare ITO electrode (i), CH/ITO electrode (ii), *n*-$NiFe_2O_4$–CH/ITO electrode (iii), and ChEt–ChOx/*n*-$NiFe_2O_4$–CH/ITO bioelectrode (iv). (c) Cyclic voltammogram of ChEt–ChOx/*n*-$NiFe_2O_4$–CH/ITO bioelectrode on increasing scan rate from 10 to 100 mV/s. (d) Magnitude of current vs potential difference as a function of square root of scan rate (10–100 mV/s).

dx.doi.org/10.1021/jp312698g | J. Phys. Chem. C 2013, 117, 8491–8502

current of the n-$NiFe_2O_4$−CH/ITO electrode (0.52 mA) is found to increase (curve iii) due to higher electron mobility resulting in improved electron transfer. The magnitude of current response further increases to 0.61 mA for ChEt−ChOx/n-$NiFe_2O_4$−CH/ITO bioelectrode (curve iv) indicating that n-$NiFe_2O_4$−CH/ITO electrode provides native microenvironment for immobilization of ChEt and ChOx resulting in enhanced electron transfer between enzyme and the electrode. The results of differential pulse voltammetric (DPV) studies reveal similar behavior of the redox potential toward the ChEt−ChOx/n-$NiFe_2O_4$−CH/ITO modified electrode as shown in Figure 4b.

Figure 4c shows CV spectra obtained of the ChEt−ChOx/n-$NiFe_2O_4$−CH/ITO bioelectrode in PBS (pH 6.4), observed as a function of scan rate (10−100 mV/s). Figure 4d reveals that both anodic (Ipa) and cathodic (Ipc) peak currents increase linearly with the square root of scan rate, $\upsilon^{1/2}$ and the observed potential peak shift (ΔEp = Epa −Epc) exhibits a linear relationship (Supporting Information Figure S3) with scan rate suggesting that the electrochemical reaction at the electrode is a diffusion controlled process, wherein electrons are transferred to and from the redox centers of the n-$NiFe_2O_4$−CH/ITO electrode indicating diffusion.[42] The observed linear dependence of peak height with sweep rate (with a linear regression coefficient of 0.979) indicates improved electrocatalytic behavior.

The surface concentration of the electrodes can be calculated from the following relation of Brown−Anson model.[7]

$$I_p = \frac{n^2F^2I^*AV}{4RT} \tag{7}$$

where n is the number of electrons transferred (1), F is the Faraday constant (96485 C/mol), I^* is the surface concentration of the corresponding electrode (mol cm^{-2}), A is the surface area of the electrode (0.25 cm^2), V is the scan rate (20 mV/s), R is the gas constant (8.314 J mol^{-1} K^{-1}) and T is the room temperature (300 K). The surface concentration of ChEt−ChOx/n-$NiFe_2O_4$−CH/ITO bioelectrode (1.29×10^{-10} mol cm^{-2}) is higher than that of the n-$NiFe_2O_4$−CH/ITO electrode (1.12×10^{-10} mol cm^{-2})/ CH/ITO (5.18×10^{-11} mol cm^{-2})/ bare ITO (2.89×10^{-11} mol cm^{-2}) electrode.

The diffusion coefficient value (D) of the ChEt−ChOx/n-$NiFe_2O_4$−CH/ITO bioelectrode has been estimated from Randles−Sevcik equation:[42,16]

$$Ip = (2.69 \times 10^5)n^{3/2}AD^{1/2}CV^{1/2} \tag{8}$$

Here I_p is peak current of the bioelectrode (I_{pa} anodic and I_{pc} cathodic), n is the number of electrons involved or electron stoichiometry (1), A is the surface area of the bioelectrode (0.25 cm^2), D is diffusion coefficient, C is surface concentration in mol (5 mM) and V is the scan rate (20 mV/s). The D value has been obtained as 1.61×10^{-4} cm^2 s^{-1}.

Electrochemical Impedance Spectroscopic (EIS) Studies. EIS studies have been performed to measure impedance changes of the electrode surface during the modification process. Nyquist plot commonly includes a semicircle region lying on the axis followed by a straight line. The semicircular part seen at higher frequencies corresponds to the electron-transfer-limited process and its diameter is equal to the charge transfer resistance (R_{ct}), which controls electron transfer kinetics of the redox probe at the electrode interface. Figure 5a displays EIS observed for bare ITO, CH/ITO, n-$NiFe_2O_4$−CH/ITO electrode and ChEt−ChOx/n-$NiFe_2O_4$−CH/ITO bioelectrode in phosphate buffer (50 mM, pH 6.4, 0.9% NaCl) containing $[Fe(CN)_6]^{3-/4-}$ (5 mM) in the frequency range, 0.00−10^7 Hz. It can be seen from the Nyquist plots that semicircle of the bare ITO electrode (R_{ct} =4.92 KΩ, curve i), characteristic of a diffusion limiting step of the electrochemical process, decreases for CH/ITO film (R_{ct} =2.60 KΩ, curve ii), and it further decreases for the n-$NiFe_2O_4$−CH/ITO nanobiocomposite film (R_{ct} =0.80 KΩ, curve iii). These results suggest that electron transfer in the n-$NiFe_2O_4$−CH/ITO nanobiocomposite film is easier between solution and the electrode, i.e., $NiFe_2O_4$ nanoparticles not only provide the hydrophilic surface, but also promote electron transfer due to permeable structure of CH/ITO electrode. However, on immobilization of ChEt and ChOx onto n-$NiFe_2O_4$−CH/ITO electrode, the semicircle part of the bioelectrode further decreases (Rct =0.54 KΩ, curve iv). This suggests that the n-$NiFe_2O_4$−CH/ITO electrode provides desired microenvironment for enzyme loading resulting in high electron pathways between electrode and the electrolyte resulting in improved diffusion of ferricyanide molecules toward the electrode surface.[43]

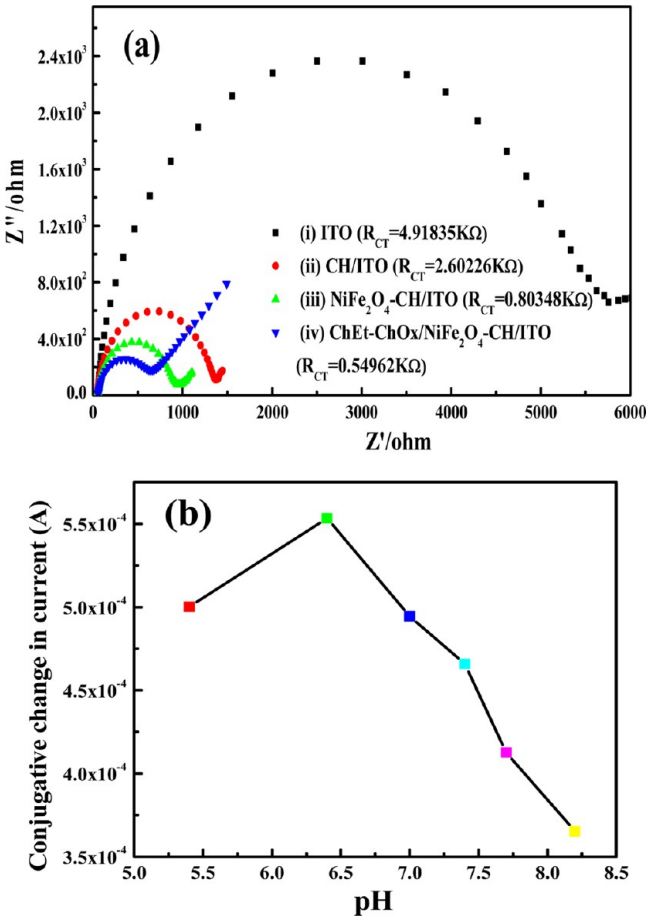

Figure 5. (a) EIS of bare ITO electrode (i), CH/ITO electrode (ii), n-$NiFe_2O_4$−CH/ITO electrode (iii), and ChEt−ChOx/n-$NiFe_2O_4$−CH/ITO bioelectrode (iv) and (b) change of conjugative current response as a function of pH ranging from 5.4 to 8.2 on ChEt−ChOx/n-$NiFe_2O_4$−CH/ITO bioelectrode.

Effect of pH and Working Potential. The pH value of the electrolyte is important for the performance of the biosensor since activity of the enzyme is greatly affected by acidity of the

dx.doi.org/10.1021/jp312698g | J. Phys. Chem. C 2013, 117, 8491−8502

medium.[7] The effect of solution pH on the electrochemical behavior of ChEt−ChOx/*n*-$NiFe_2O_4$−CH/ITO has been investigated by CV in PBS (50 mM, 0.9% NaCl) containing $[Fe(CN)_6]^{3-/4-}$ (5 mM) at 20 mV/s scan rate shown in the Supporting Information (Figure S4). The results show variation of the CV peak current response of the ChEt−ChOx/*n*-$NiFe_2O_4$−CH/ITO bioelectrode at different pH 5.4−8.2 in presence of the same concentration of cholesterol oleate. The maximum magnitude of current is obtained at pH 6.4 (Figure 5b) indicating that the ChEt−ChOx/*n*-$NiFe_2O_4$−CH/ITO bioelectrode is most active at pH 6.4 at which ChOx and ChEt retain their natural structures. The presence of strong acidic or alkaline environments would result in denaturation of the enzyme. Therefore, pH 6.4 is selected as the optimum value of pH for the fabricated biosensor.

The effect of working potential on the performance of the bioelectrode has been investigated from 0.1 to 0.8 V in the presence of cholesterol oleate (200 mg/dL) and a PBS (50 mM, pH 6.4, 0.9% NaCl) containing 5 mM $[Fe(CN)_6^{3-/4-}]$. The steady-state current response increases with the working potential from 0.3 to 0.5 V and it then increases smoothly from 0.5 to 0.8 V (data not shown). Therefore, 0.5 V is selected as the working potential for amperometric for amperometric detection of total cholesterol concentration.

Electrochemical Response Studies of ChEt−ChOx/*n*-$NiFe_2O_4$−CH/ITO Bioelectrode. Figure 6a shows the electrochemical response of ChEt−ChOx/*n*-$NiFe_2O_4$−CH/ITO bioelectrode obtained as a function of cholesterol concentration (0−500 mg/dL) using CV technique in PBS (50 mM, 0.9% NaCl) containing $[Fe(CN)_6]^{3-/4-}$ (5 mM) as mediator at scan rate of 20 mV/s.

The oxidation peak seen at 0.35 V corresponds to the oxidation of H_2O_2 arising due to the enzymatic reaction between enzyme (ChEt−ChOx) and cholesterol oleate. The increase in value of the oxidation current with increasing cholesterol oleate concentration (5−500 mg/dL) results in increased concentration of H_2O_2 during the enzymatic reaction. This may perhaps be due to well-aligned cubic spinel network of *n*-$NiFe_2O_4$ nanoparticles that act as good acceptor of electrons (generated during reoxidation of enzyme) that are transferred to electrode via Ni^{2+}/Fe^{3+} redox couple resulting in increased electrochemical current response. The calibration curve (Figure 6b), shows that magnitude of the oxidation peak current increases linearly with increasing concentration of cholesterol oleate. As can be seen, the response current enhances as the concentration of cholesterol increases and saturates at high concentration of cholesterol. Under optimized conditions, the steady-state current of the fabricated cholesterol biosensor shows a linear range from 5 to 400 mg/dL with linear regression coefficient of 0.9801. The sensitivity of the ChEt−ChOx/*n*-$NiFe_2O_4$−CH/ITO bioelectrode obtained from the slope of the curve is found to be as 1.703 μA/(mg/dL cm^{-2}). The standard deviation and low detection limit for the bioelectrode have been found to be as 13.8864 μA and 24.46 mg/dL cm^{-2}, respectively. The response time of the ChEt−ChOx/*n*-$NiFe_2O_4$−CH/ITO bioelectrode has been measured to be as 15 s and is attributed to faster electron communication feature of *n*-$NiFe_2O_4$−CH/ITO electrode. The desired total plasma cholesterol for an individual is known to be less than 5.2 mM (200 mg/dL), with the high level of cholesterol being considered as greater than 6.2 mM (240 mg/dL). The fabricated biosensor covers a wide range of cholesterol concentration, promising for the clinical diagnostics of total cholesterol.

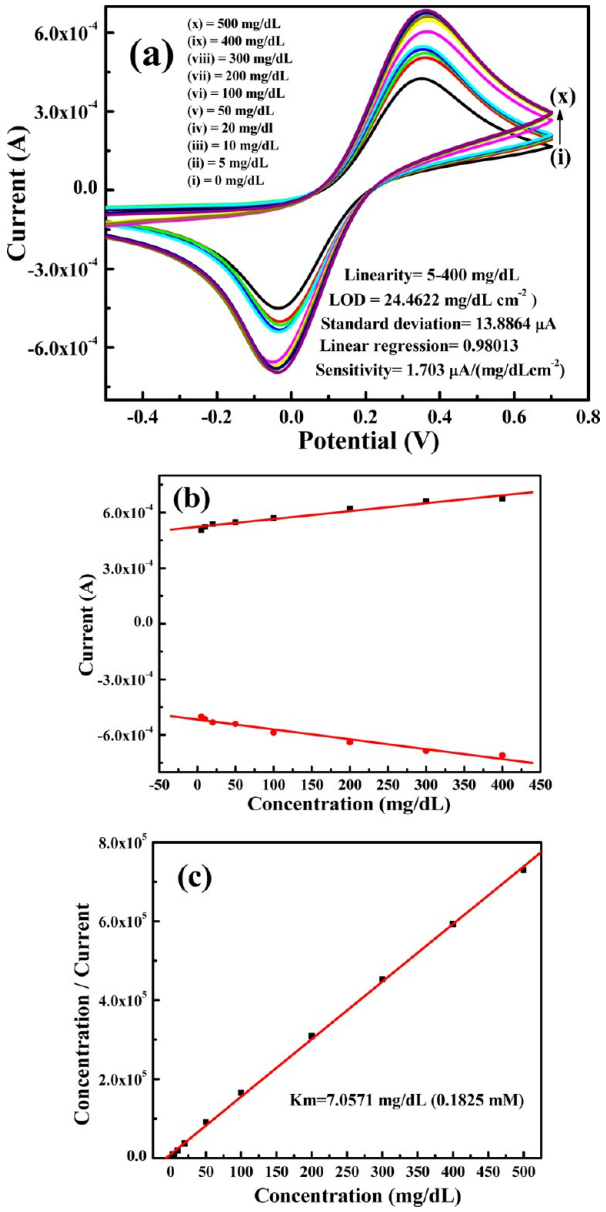

Figure 6. (a) Electrochemical response of ChEt−ChOx/*n*-$NiFe_2O_4$−CH/ITO bioelectrode with respect to cholesterol oleate concentration (5−500 mg/dL) in phosphate buffer (50 mM, pH 6.4, 0.9% NaCl) containing 5 mM $[Fe(CN)_6]^{3-/4-}$ at the scan rate of 20 mV/s . (b) Calibration curve of the variation in current as a function of cholesterol oleate concentration and (c) Hanes plot between the substrate concentration and substrate concentration/current.

The Michaelis−Menten constant (K_m) for the ChEt−ChOx/*n*-$NiFe_2O_4$−CH/ITO bioelectrode, estimated by Hanes plot i.e. graph between [substrate concentration] and [substrate concentration/current] (Figure 6c) has been found to be as 7.0571 mg/dL (0.18 mM). The value of K_m depends on various factors such as the nature of matrix and the method of immobilization of enzymes, that may bring different conformational changes in the enzyme structure as the enzyme kinetics is environment sensitive.[44] The small K_m value indicates high affinity of the immobilized enzymes of ChEt−ChOx/*n*-$NiFe_2O_4$−CH/ITO bioelectrode that is attributed to favorable conformation of ChEt and ChOx and higher loading onto *n*-

dx.doi.org/10.1021/jp312698g | J. Phys. Chem. C 2013, 117, 8491−8502

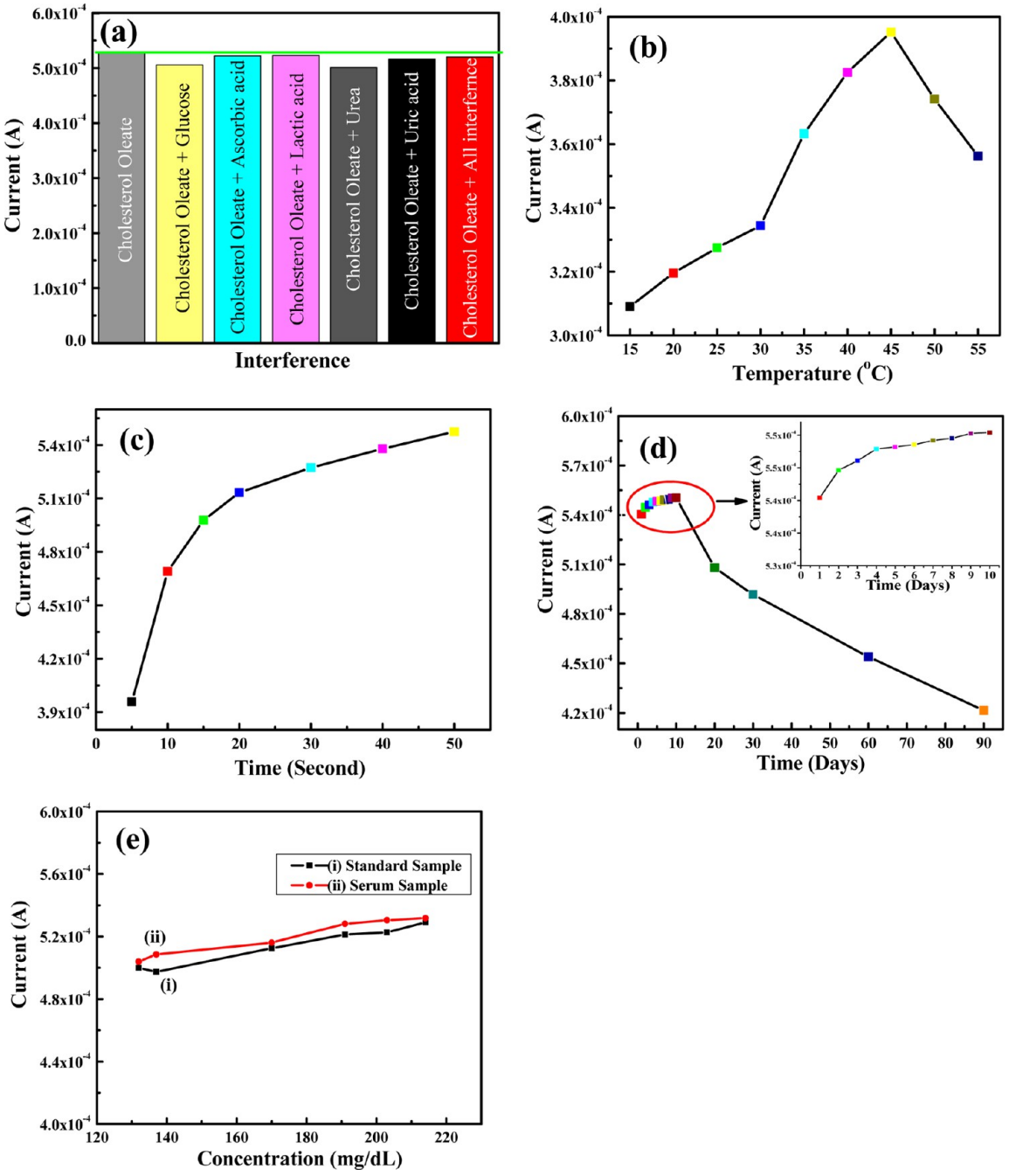

Figure 7. (a) Effect of interferents, on electrctrochemical response of ChEt−ChOx/*n*-$NiFe_2O_4$−CH/ITO bioelectrode (inset bar graph of different interferents). (b) Effect of temperature on ChEt−ChOx/*n*-$NiFe_2O_4$−CH/ITO bioelectrode from 15 to 55 °C. (c) Electrochemical response time from 5 to 50s incubation period. (d) Shelf life curve for ChEt−ChOx/*n*-$NiFe_2O_4$−CH/ITO bioelectrode as a function of day. (e) Determination of cholesterol concentration: (i) prepared standard cholesterol solution and (ii) cholesterol concentration in serum samples.

$NiFe_2O_4$−CH/ITO electrode surface. This nanostructured matrix provides high electron communication between the enzyme's active site and the electrode along with high surface area providing a suitable native environment that helps in effective immobilization of enzyme in large amount on the surface of the matrix. Moreover, majority of the matrices used for fabrication of biosensors require cross-linkers for enzyme immobilization. However, this is not a necessity for the metal oxide based matrix, used in the present study, owing to its high IEP (e.g., Ni and Fe oxide have IEP varying from 6.6 to 10.7) which make it suitable for immobilization.

Enzyme Activity Studies. The apparent enzyme activity (U cm^{-2}) is defined as one unit of enzyme activity that results in the conversion of 1 μmol of cholesterol into cholest-4-ene-3-one per minute. It can be estimated using the method based on the difference of absorbance observed before and after the incubation of enzyme bound electrode.[31] The apparent enzyme activity is evaluated using the following equation.

$$\alpha_{app}^{enz}\ (\mathrm{U\ cm^{-2}}) = AV/\varepsilon ts \tag{9}$$

Here A is the difference in absorbance before and after incubation, V is the total volume (3.08 cm^3), ε is the millimolar

dx.doi.org/10.1021/jp312698g | J. Phys. Chem. C 2013, 117, 8491−8502

extinction coefficient (7.5 for *o*-dianisidine at 500 nm), *t* is the reaction time (min), and *s* is the surface area (0.25 cm^2) of the electrode. For measurement, a solution of 20 μL of HRP, 10 μL of dye (*o*-dianisidine), and 50 μL of 200 mg/dL cholesterol oleate is diluted by adding 3 mL of PBS (pH = 7.0) and is kept in a thermostat at 25 °C. The ChEt−ChOx/*n*-$NiFe_2O_4$−CH/ITO bioelectrode is incubated in PBS for about 3 min after which, this bioelectrode is removed and the absorbance of the solution is measured at 500 nm using a double beam spectrophotometer to estimate the concentration of product produced as a result of enzymatic reaction. The apparent enzyme activity has been found to be as 0.6038 U cm^{-2} indicating that 0.6038 units of enzyme per cm^2 actively participate in the enzymatic reaction.

Effect of Interferents, Thermal Stability, Response Time, Stability, and Reproducibility of the ChEt−ChOx/*n*-$NiFe_2O_4$−CH/ITO Bioelectrode. The influence of common interferents on the fabricated ChEt−ChOx/*n*-$NiFe_2O_4$−CH/ITO bioelectrode has been determined in PBS (50 mM, pH 6.4, 0.9% NaCl) containing $[Fe(CN)_6]^{3-/4-}$ (5 mM) at 20 mV/s scan rate using CV technique shown in the Supporting Information (Figure S5). The change in electrochemical current response has been measured in PBS containing equal amount (1:1) standard cholesterol oleate (200 mg/dL) solution along with normal physiological concentration of different interferents such as glucose (5 mM), urea (1 mM), lactic acid (LA, 0.5 mM), uric acid (UA, 0.1 mM) and ascorbic acid (AA, 0.05 mM). The value of oxidation peak current decreases by 4.24%, 1.33%, 1%, 5.33%, 2.36%, and 1.65% on addition of glucose, AA, LA, urea, UA, and mixture of these interferents, respectively shown in the bar graph of Figure 7a. These results indicate that response of ChEt−ChOx/*n*-$NiFe_2O_4$−CH/ITO bioelectrode does not significantly get affected due to presence of these interferents.

The thermal stability of the ChEt−ChOx/*n*-$NiFe_2O_4$−CH/ITO bioelectrode has been studied by measuring the current response at different temperatures ranging from 15 to 55 °C (Figure 7b). It can be seen that the amperometric current response of the modified bioelectrode is enhanced with increasing temperature up to 45 °C, and then goes down as the temperature turns higher. This phenomenon may be attributed to the fact that the enzyme is denatured at high temperature.[7]

For the determination of response time (Figure 7c) of ChEt−ChOx/*n*-$NiFe_2O_4$−CH/ITO bioelectrode, amperometric current response is measured from 5 to 50 s. The magnitude of current increases initially (5−15 s) and after 15 s, it becomes almost constant indicating that 15 s is the response time of ChEt−ChOx/*n*-$NiFe_2O_4$−CH/ITO bioelectrode.

The reproducibility of the proposed cholesterol biosensor has been studied. Repetitive measurements have been carried out in 10 mL PBS containing 200 mg/dL cholesterol oleate. The currents obtained in 15 repeated measurements show a RSD of 2−3%, confirming that the obtained data are reproducible. Thus, the *n*-$NiFe_2O_4$−CH/ITO electrode efficiently retains enzyme activity and the fabricated cholesterol biosensor has a good reproducibility.

The shelf life of ChEt−ChOx/*n*-$NiFe_2O_4$−CH/ITO bioelectrode (Figure 7d) has been determined by measuring electrochemical current response of a 200 mg/dL standard cholesterol oleate solution at regular intervals of 1 day up to 10 days and then after a gap of 10 days. It has been found that the bioelectrode retains its enzyme activity up to 94% after 20 days, 91% after 30 days, and 84% after 60 days and falls to 78% after 90 days when stored under refrigerated condition (4 °C). The high stability can be attributed to the use of chitosan and the *n*-$NiFe_2O_4$ network. Since chitosan in aqueous solvent is protonated and is positively charged, it can thus be strongly adsorbed onto the *n*-$NiFe_2O_4$ network. The interaction between *n*-$NiFe_2O_4$ and chitosan results in increased retention of enzymes on the surface. In addition, *n*-$NiFe_2O_4$ can strongly adsorb enzymes and prevent the leakage of the immobilized enzymes.[45,46] The high sensitivity and high stability of the fabricated biosensor indicates that the *n*-$NiFe_2O_4$ network structure along with chitosan provides an excellent biocompatible microenvironment for the immobilization of the enzymes.

Response of ChEt−ChOx/*n*-$NiFe_2O_4$−CH/ITO Bioelectrode with Serum Samples. Attempts have been made to estimate total cholesterol using ChEt−ChOx/*n*-$NiFe_2O_4$−CH/ITO bioelectrode in serum samples obtained from a clinic located in New Delhi, India. During these experiments, the ChEt−ChOx/*n*-$NiFe_2O_4$−CH/ITO bioelectrode is dipped in PBS containing serum samples and response current is observed using CV technique at 20 mV/s scan rate (Figure 7e). It can be seen (Table 2) that magnitude of the current obtained with serum samples and prepared standard cholesterol oleate solution is in reasonable agreement, indicating that cholesterol biosensor has a great potential for practical application for the analysis of total cholesterol in real clinical samples. Table S6 (Supporting Information) contains results of the studies using the ChEt−ChOx/*n*-$NiFe_2O_4$−CH/ITO bioelectrode including others reported in the literature.

Table 2. Determination of Total Cholesterol in Serum Samples

cholesterol concentration (mg/dL)	value of current obtained with serum sample (mA)	value of current obtained for pure cholesterol oleate sample (mA)	% RSD
132	0.503 961	0.500 027	0.79
137	0.508 55	0.497 405	2.24
170	0.516 089	0.512 483	0.70
191	0.528 216	0.521 333	1.32
203	0.530 511	0.522 644	1.51
214	0.531 822	0.5292	0.50

CONCLUSIONS

A novel biocompatible and antimicrobial cholesterol biosensor has been fabricated by immobilizing ChOx and ChEt on the surface of *n*-$NiFe_2O_4$ magnetic nanoparticles (~16−32 nm) synthesized by hydrothermal route. The ChEt−ChOx/*n*-$NiFe_2O_4$−CH/ITO bioelectrode shows rapid response (15 s), high sensitivity of 1.703 μA/(mg/dL cm^{-2}), broad linear range (5−400 mg/dL), standard deviation (13.8864 μA), low detection limit (24.46 mg/dL cm^{-2}), good reproducibility and long-term stability. The wide detection range and high sensitivity have been assigned to the enhanced current response arising due to presence of the monodispersed *n*-$NiFe_2O_4$ nanoparticles in chitosan matrix and its good biocompatibility and antimicrobial behavior maintain biological activity of the immobilized enzymes and facilitates electron transfer produced in the enzymatic reaction. The low value of Michaelis−Menten constant of 0.18 mM indicates high enzyme affinity to cholesterol. Moreover, this total cholesterol biosensor virtually eliminates role of other analytes present in the serum samples.

dx.doi.org/10.1021/jp312698g | J. Phys. Chem. C 2013, 117, 8491−8502

The results clearly suggest that antimicrobial and biocompatible n-$NiFe_2O_4$−CH nanocomposite is a promising platform for the development of other *in vitro*/*in vivo* biosensors, biomolecular electronic devices. The challenge is to develop suitable scalable nanofabrication method for commercialization of the n-$NiFe_2O_4$−CH nanocomposite for other biomedical and nanobioelectronics applications.

■ ASSOCIATED CONTENT

Supporting Information

Antimicrobial activity test and bioassay of CH, n-$NiFe_2O_4$/CH, and ChEt−ChOx/n-$NiFe_2O_4$/CH solution against with different microorganisms/algae/fungi, magnitude of potential difference observed as a function of scan rate (10−100 mV/s) and CV studies of the ChEt−ChOx/n-$NiFe_2O_4$−CH/ITO bioelectrode as a function of pH ranging from 5.4 to 8.2, effect of interferents on the electrctrochemical response of the ChEt−ChOx/n-$NiFe_2O_4$−CH/ITO bioelectrode, and biosensing characteristics of the ChOx−ChEt/n-$NiFe_2O_4$−CH/ITO bioelectrode along with those reported in the literature for total cholesterol estimation. This material is available free of charge via the Internet at http://pubs.acs.org.

■ AUTHOR INFORMATION

Corresponding Author

*(B.D.M.) E-mail: bansi.malhotra@gmail.com. Telephone: +91-11-27294668. Fax: 91-11-27871023.

Notes

The authors declare no competing financial interest.

■ ACKNOWLEDGMENTS

We thank the Director, National Physical Laboratory, New Delhi, India, for providing the facilities. We acknowledge the financial support received under the Department of Science & Technology [DST/TSG/ME/2008/18), Govt. of India, project], the in-house NPL project (OLP-070632D), and the Indian Council of Medical Research (ICMR/RHN/ADHOC/5/2012-2013). J.S. is thankful to the Council of Scientific & Industrial Research (CSIR) India for the award of Research Associateship and financial support received under World Class University (WCU) programs (R31-20029) funded by MEST, Republic of Korea. A.R. is thankful to Indian Council of Medical Research (ICMR) for the award of Project Associateship. B.D.M thanks the Ministry of Education, Science and Technology (*R*32−20026) of Korea for the opportunity provided during his visit to the Chungnam National University as visiting professor under the World Class University project during June−July 2012 and March 2013.

■ REFERENCES

(1) Zhuo, Y.; Yuan, P. X.; Yuan, R.; Chai, Y. Q.; Hong, C. L. Bienzyme Functionalized Three-Layer Composite Magnetic Nanoparticles for Electrochemical Immunosensors. *Biomaterials* **2009**, *30*, 2284−2290.

(2) Luo, L.; Zhu, L.; Xu, Y.; Shen, L.; Wang, X.; Ding, Y.; Li, Q.; Deng, D. Hydrogen Peroxide Biosensor Based on Horseradish Peroxidase Immobilized on Chitosan-Wrapped $NiFe_2O_4$ Nanoparticles. *Microchim. Acta* **2011**, *174*, 55−61.

(3) Kalita, P.; Singh, J.; Singh, M. K.; Solanki, P. R.; Sumana, G.; Malhotra, B. D. Ring Like Self Assembled Ni Nanoparticles based Biosensor for Food Toxin Detection. *Appl. Phys. Lett.* **2012**, *100*, 093702.

(4) Kaushik, A.; Khan, R.; Solanki, P. R.; Pandey, P.; Alam, J.; Ahmad, S.; Malhotra, B. D. Iron Oxide Nanoparticles−Chitosan Composite Based Glucose Biosensor. *Biosens. Bioelectron.* **2008**, *24*, 676−683.

(5) Gŏımez-Hens, A.; Fernăındez-Romero, J. M.; Aguilar-Caballos, M. P. Nanostructures as Analytical Tools in Bioassay. *Trends Anal. Chem.* **2008**, *27*, 394−406.

(6) Ansari, A. A.; Kaushik, A.; Solanki, P. R.; Malhotra, B. D. Sol−gel Derived Nanoporous Cerium Oxide Film for Application to Cholesterol Biosensor. *Electrochem. Commun.* **2008**, *10*, 1246−1249.

(7) Singh, J.; Kalita, P.; Singh, M. K.; Malhotra, B. D. Nanostructured Nickel Oxide-Chitosan Film for Application to Cholesterol Sensor. *Appl. Phys. Lett.* **2011**, *98*, 123702.

(8) Aravamudhan, S.; Ramgir, N. S.; Bhansali, S. Sensitive Estimation of Total Cholesterol in Blood Using Au Nanowires Based Micro-Fluidic Platform. *Sens. Actuators. B* **2007**, *127*, 29−35.

(9) Willner, I.; Katz, E. Integration of Layered Redox-Proteins and Conductive Supports for Bioelectronics Applications. *Angew. Chem., Int. Ed.* **2000**, *39*, 1180−1218.

(10) Sarma, A. K.; Vatsyayan, P.; Goswami, P.; Minteer, S. D. Recent Advances in Material Science for Developing Enzyme Electrodes. *Biosens. Bioelectron.* **2009**, *24*, 2313−2322.

(11) Lin, C. C.; Yang, M. C. Cholesterol Oxidation Using Hollow Fiber Dialyzer Immobilized with Cholesterol Oxidase: Effect of Storage and Reuse. *Biomaterials* **2003**, *24*, 549−557.

(12) Yapar, E.; Kayahan, S. K.; Bozkurt, A.; Toppare, L. Immobilizing Cholesterol Oxidase in Chitosan−Alginic Acid Network. *Carbohydr. Polym.* **2009**, *76*, 430−436.

(13) Reiss, G.; Hütten, A. Magnetic nanoparticles: Applications beyond Data Storage. *Nat. Mater.* **2005**, *4*, 725−726.

(14) Beveridge, J. S.; Stephens, J. R.; Williams, M. E. The Use of Magnetic Nanoparticles in Analytical Chemistry. *Annu. Rev. Anal. Chem.* **2011**, *4*, 251−273.

(15) Jung, J. H.; Lee, J. H.; Shinkai, S. Functionalized Magnetic Nanoparticles as Chemosensors and Adsorbents for Toxic Metal Ions in Environmental and Biological Fields. *Chem. Soc. Rev.* **2011**, *40*, 4464−4474.

(16) Solanki, P. R.; Kaushik, A.; Agrawal, V. V.; Malhotra, B. D. Nanostructured Metal Oxide-Based Biosensors. *NPG Asia Mater.* **2011**, *3*, 17−24.

(17) Colombo, M.; Carregal-Romero, S.; Casula, M. F.; Gutiérrez, L.; Morales, M.; Böhm, I. B.; Heverhagen, J. T.; Prosperi, D.; Parak, W. J. Biological Applications of Magnetic Nanoparticles. *Chem. Soc. Rev.* **2012**, *41*, 4306−4334.

(18) Laokul, P.; Amornkitbamrung, V.; Seraphin, S.; Maensir, S. Characterization and Magnetic Properties of Nanocrystalline $CuFe_2O_4$, $NiFe_2O_4$, $ZnFe_2O_4$ Powders Prepared by the Aloe Vera Extract Solution. *Curr. Appl. Phys.* **2011**, *11*, 101−108.

(19) Zhang, D. G.; Tong, Z. W.; Xu, G. Y.; Li, S. Z.; Ma, J. J. Templated Fabrication of $NiFe_2O_4$ Nanorods: Characterization, Magnetic and Electrochemical Properties. *Solid State Sci.* **2009**, *11*, 113−117.

(20) Srivastava, M.; Ojha, A. K.; Chaubey, S.; Materny, A. Synthesis and Optical Characterization of Nanocrystalline $NiFe_2O_4$ Structures. *J. Alloys Compd.* **2009**, *481*, 515−519.

(21) Fan, G.; Xiang, X.; Fan, J.; Li, F. Template-Assisted Fabrication of Macroporous $NiFe_2O_4$ Films with Tunable Microstructural, Magnetic and Interfacial Properties. *J. Mater. Chem.* **2010**, *20*, 7378−7385.

(22) Cıner, F. Y.; Evik, E. C.; Enel, M. S.; Baykal, A. U. Development of an Amperometric Hydrogen Peroxide Biosensor Based on The Immobilization of Horseradish Peroxidase onto Nickel Ferrite Nanoparticle-Chitosan Composite. *Nano-Micro Lett.* **2011**, *3*, 91−98.

(23) Fang, B.; Feng, Y.; Liu, M.; Wang, G.; Zhang, X.; Wang, M. Electrocatalytic Oxidation of Hydrazine at a Glassy Carbon Electrode Modified with Nickel Ferrite and Multi-Walled Carbon Nanotubes. *Microchim. Acta.* **2011**, *175*, 145−150.

(24) Satyanarayana, L.; Reddy, K. M.; Manorama, V. Nanosized Spinel $NiFe_2O_4$: A Novel Material for the Detection of Liquefied Petroleum Gas in Air. *Mater. Chem. Phys.* **2003**, *82*, 21−26.
(25) Luo, L. Q.; Li, Q. X.; Xu, Y. H.; Ding, Y. P.; Wang, X.; Deng, D. M.; Xu, Y. J. Amperometric Glucose Biosensor Based on $NiFe_2O_4$ Nanoparticles and Chitosan. *Sens. Actuators B* **2010**, *145*, 293−298.
(26) Singh, J.; Srivastava, M.; Roychoudhury, A.; Lee, D. W.; Lee, S. H.; Malhotra, B. D. Bienzyme-Functionalized Monodispersed Biocompatible Cuprous Oxide/Chitosan Nanocomposite Platform for Biomedical Application. *J. Phys. Chem. B* **2013**, *117*, 141−152.
(27) Bae, S.; Lee, S. W.; Takemura, Y. Applications of $NiFe_2O_4$ Nanoparticles for a Hyperthermia Agent in Biomedicine. *Appl. Phys. Lett.* **2006**, *89*, 252503.
(28) Pradhan, S. K.; Bid, S.; Gateshki, M.; Petkov, V. Microstructure Characterization and Cation Distribution of Nanocrystalline Magnesium Ferrite Prepared by Ball Milling. *Mater. Chem. Phys.* **2005**, *93*, 224−230.
(29) Srivastava, M.; Chaubey, S.; Ojha, A. K. Investigation on Size Dependent Structural and Magnetic Behavior of Nickel Ferrite Nanoparticles Prepared by Sol−Gel and Hydrothermal Methods. *Mater. Chem. Phys.* **2009**, *118*, 174−180.
(30) Pradeep, A.; Priyadharsini, P.; Chandrasekaran, G. Sol−gel Route of Synthesis of Nanoparticles of $MgFe_2O_4$ and XRD, FTIR and VSM Study. *J. Magn. Magn. Mater.* **2008**, *320*, 2774−2779.
(31) Xia, B.; Lenggoro, I. W.; Okuyam, K. Preparation of Nickel Powders by Spray Pyrolysis of Nickel Formate. *J. Am. Ceram. Soc.* **2001**, *84*, 1425−1432.
(32) Byrappa, K. *J.* Novel Hydrothermal Solution Routes of Advanced High Melting Nanomaterial Processing. *Ceram. Soc. Jpn.* **2009**, *117*, 236−244.
(33) Sayed, A. M. E. Influence of Zinc Content on Some Properties of Ni−Zn Ferrites. *Ceram. Int.* **2002**, *28*, 363−367.
(34) Maaz, K.; Mumtaz, A.; Hasanain, S. K.; Bertino, M. F. Temperature Dependent Coercivity and Magnetization of Nickel Ferrite Nanoparticles. *J. Magn. Magn. Mater.* **2010**, *322*, 2199−2202.
(35) Varadwaj, K. S. K.; Panigrahi, M. K. Ghose Effect of Capping and Particle Size on Raman Laser-Induced Degradation of γ-Fe_2O_3 Nanoparticles. *J. Solid State Chem.* **2004**, *177*, 4286−4292.
(36) Qu, Y.; Yang, H.; Yang, N.; Fan, Y.; Zhu, H.; Zou, G. The Effect of Reaction Temperature on the Particle Size, Structure and Magnetic Properties of Co- Precipitated $CoFe_2O_4$ Nanoparticles. *Mater. Lett.* **2006**, *60*, 3548−3552.
(37) Kreisel, J.; Lucazeau, G.; Vincent, H. Raman Spectra and Vibrational Analysis of $BaFe_{12}O_{19}$ Hexagonal Ferrite. *J. Solid State Chem.* **1998**, *137*, 127−137.
(38) Kamnev, A. A.; Ristic, M. Fourier Transform Far-Infrared Spectroscopic Evidence For the Formation of a Nickel Ferrite Precursor in Binary Ni(II)-Fe(III) Hydroxides on Coprecipitation. *J. Mol. Struct.* **1997**, *409*, 301−304.
(39) Kim, J. H.; Hwang, I. S. Development of an in Situ Raman Spectroscopy System for Surface Oxide Films on Metals and Alloys in High Temperature Water. *Nucl. Eng. Des.* **2005**, *235*, 1029−1040.
(40) De Paiva, J. A. C.; Graca, M. P. F.; Monteiro, J.; Macedo, M. A.; Valente, M. A. Spectroscopy Studies of $NiFe_2O_4$ Nanosized Powders Obtained Using Coconut Water. *J. Alloys Compd.* **2009**, *485*, 637−641.
(41) Hanh, N.; Quy, O. K.; Thuy, N. P.; Tung, L. D.; Spinu, L. Synthesis of Cobalt Ferrite Nanocrystallites by the Forced Hydrolysis Method and Investigation of Their Magnetic Properties. *Physica B* **2003**, *327*, 382−384.
(42) Shan, D.; Yao, W.; Xue, H. Electrochemical Study of Ferrocenemethanol-Modified Layered Double Hydroxides Composite Matrix: Application to Glucose Amperometric Biosensor. *Biosens. Bioelectron.* **2007**, *23*, 432−437.
(43) Zhang, H. L.; Zou, X. Z.; Lai, G. S.; Han, D. Y.; Wang, F. Direct Electrochemistry of Hemoglobin Immobilized on Carbon-Coated Iron Nanoparticles for Amperometric Detection of Hydrogen Peroxide. *Electroanalysis* **2007**, *19*, 1869−1874.
(44) Topoglidis, E.; Astuti, Y.; Duriaux, F.; Gratzel, M.; Durrant, J. R. Direct Electrochemistry and Nitric Oxide Interaction of Heme Proteins Adsorbed on Nanocrystalline Tin Oxide Electrodes. *Langmuir* **2003**, *19*, 6894−6900.
(45) Luo, X. L.; Xu, J. J.; Du, Y.; Chen, H. Y. A Glucose Biosensor Based on Chitosan−Glucose Oxidase−Gold Nanoparticles Biocomposite Formed by One-Step Electrodeposition. *Anal. Biochem.* **2004**, *334*, 284−289.
(46) Singh, J.; Srivastava, M.; Kalita, P.; Malhotra, B. D. A Novel Ternary $NiFe_2O_4$/CuO/FeO-Chitosan Nanocomposite as a Cholesterol Biosensor. *Process Biochem.* **2012**, *47*, 2189−2198.